Thermodynamic principles of enzymatic regulation in biomolecular condensates from reaction-coupled molecular modeling

Enrico Lavagna[1], Francesco Delfino[1], Georgii Koniukov[1], Matteo Paloni[1,2], Luca Ciandrini[1,3], and Alessandro Barducci[1]

[1]CBS (Centre de Biologie Structurale), Université de Montpellier, CNRS, INSERM, Montpellier, France
[2]Department of Chemical Engineering, Thomas Young Centre, University College London, London WC1E 7JE, United Kingdom
[3]Institut Universitaire de France (IUF)

Abstract

Biomolecular condensates are dynamic cellular assemblies often regulated by energy-consuming processes such as post-translational modifications (PTMs). These reactions can act as molecular switches that control condensate assembly and dissolution, or sustain non-equilibrium steady states that support biological function. Nevertheless, how reaction dynamics couple to spatial organization at the molecular scale remains poorly understood. Here, we introduce a minimal molecular model to study enzymatic regulation of condensate assembly and structure under thermodynamic constraints. Our simulations reveal a non-monotonic dependence of condensate stability on modification strength, identifying an optimal regime for active control. We further find that chemical activity becomes spatially localized at the condensate interface, which emerges as a key reactive hub shaped by local molecular environments. Together, these results show how thermodynamically consistent, particle-based simulations can provide insight into principles of active condensate regulation at molecular resolution.

Introduction

Cellular condensates are membrane-less organelles, primarily made of proteins and nucleic acids, that take part in many vital processes throughout the nucleus and cytoplasm [1, 2, 3, 4]. Their assembly and material properties originate from a network of dynamical interactions between one or more condensate components [5, 6, 7] that is often modulated by energy-consuming processes, such as enzymatic post-translational modifications (PTMs) acting as fast regulatory switches [8, 9]. Such regulatory mechanisms can maintain condensates in non-equilibrium steady states (NESS)[10] which endow them with properties beyond passive compartmentalization [11] and possibly prevent irreversible aggregation[12]. Experimental studies have begun to dissect how ATP-dependent reactions shape condensate behavior, with effects ranging from altered morphology and phase boundaries to compositional remodeling and rheological changes [10, 13, 14, 15, 16]. These findings indicate that active regulation can control condensate properties in ways not captured by equilibrium thermodynamics. The theoretical community has explored how chemical reactions modulate phase-separated systems using mesoscale continuum descriptions [17, 18, 19, 20]. These approaches offer insight into how reaction-driven processes influence droplet size, number, and phase boundaries [21]. However, their lack of molecular resolution limits their ability to describe key physical mechanisms such as spatial correlations, interaction heterogeneity, and the microscopic organization of components within condensates. Molecular simulations have proven powerful for investigating the formation, structure, and dynamics of biomolecular condensates [22, 23, 24], and allow to bridge the gap between mesoscale theories and microscopic processes. However, applying them to systems with chemical reactions remains challenging, particularly when aiming to model reactivity in a thermodynamically consistent way. Early efforts to introduce reactive particle-based models [25, 26] provided valuable insight on the interplay of chemical activity on phase-separated systems. However, these models typically assume fixed reaction rates

and do not account for the effect that different solvents, e.g. the condensed phase, may have on reaction kinetics and enzyme efficiency. This can lead to thermodynamic inconsistencies even in equilibrium conditions, as shown by Fröhner and Noé [27], who proposed a reaction scheme obeying local detailed balance (LDB) to address this issue. A recent study by Zippo et al. [28] applied a reaction scheme consistent with local detailed balance to model progressive phosphorylation of the TDP-43 protein by the CK1δ kinase, demonstrating how incremental modification can drive the release of proteins from condensate-like assemblies. While this work illustrates how chemical reactions may modulate protein localization, our understanding of how energy-consuming processes shape the properties of non-equilibrium steady states remains limited.

To address these questions, we introduce a minimal particle-based model of a chemically regulated condensate that incorporates reactive dynamics consistent with local detailed balance. In our model, scaffold proteins can switch between a phase-separating state and a repulsive state, mimicking the action of post-translational modifications. By allowing sustained, energy-consuming conversion between these states, we explore how chemical driving controls condensate composition, spatial organization, and steady-state behavior.

Results

A Minimal Molecular Model for Biochemical Regulation of Condensates

Here, we introduce a minimal molecular model to investigate the physical basis of condensate regulation by energy-consuming reactions, while circumventing the molecular complexity of real membrane-less organelles. To this end, we adopt an ultra-coarse-grained representation in which each protein is modeled as a single particle. The system includes two molecular species: a scaffold protein that can switch between a condensate-forming (non-phosphorylated, N) state and a more soluble (phosphorylated, P) state; and a kinase enzyme (K) that catalyzes the phosphorylation reaction ($N + K \rightarrow P + K$).

Interactions between proteins are modeled via Lennard-Jones (LJ) potentials, with the interaction strength and size of the non-phosphorylated scaffold ($\varepsilon_N = 1$, $\sigma_N = 1$) defining the energy and length scales. We set the simulation temperature to $k_BT = 0.75$, so that the non-phosphorylated scaffold undergoes phase separation with an excess transfer free energy of $\Delta G_{\text{trans}} \simeq -4\,\text{kJ}\,\text{mol}^{-1}$, consistent with values measured *in vitro* for phase-separating proteins like FUS [29], DDX4 [30] and LAF-1[31].

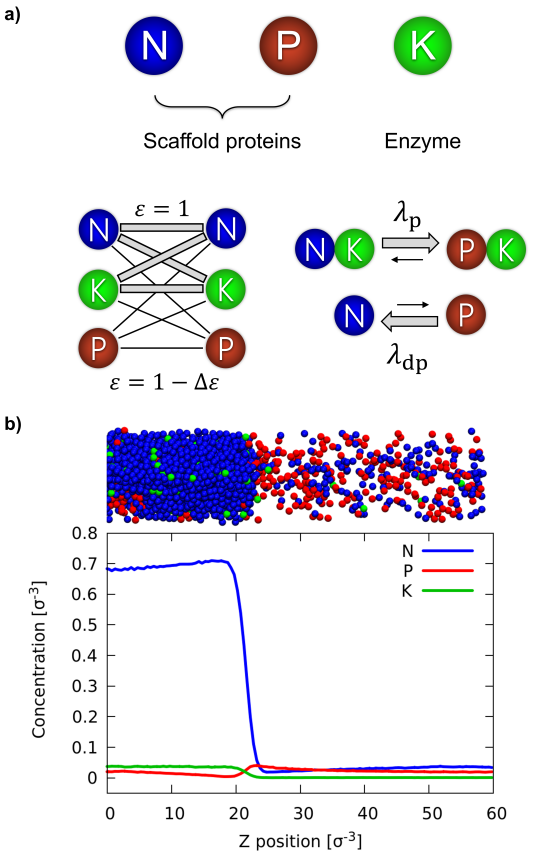

Figure 1: *Model and simulation setup.* a) Top: the three particles that make up the model. Bottom left: schematics of the interactions. Bottom right: a schematic representation of the implemented reaction cycle. b) Concentration profiles along the z coordinate of a typical slab simulation at steady state, along with a snapshot of the simulated system. Scaffold proteins are depicted in blue, phosphorylated scaffold in red, and protein kinases in green.

To model the regulatory effect of phosphorylation, we assign reduced interaction strength to the P state $\varepsilon_P \lesssim 0.69$, such that they do not phase separate at the chosen temperature. Indeed, since the critical temperature for particles interacting through a truncated and shifted LJ potential with $\varepsilon = 1$ is $k_BT = 1.08$ [32], it follows that $\varepsilon_{crit} = \frac{k_BT}{1.08}$ and in our system $\varepsilon_{crit} = \frac{0.75}{1.08} \simeq 0.69$. Kinases ($K$) are modeled as particles identical to N in terms of interaction strength, so that they co-partition into condensates, in line with *in vitro* [33] *in vivo* [9] observations. All particles are assumed to have the same size ($\sigma_N = \sigma_P = \sigma_K$), and the interaction parameters for all species are summarized in Table S2. The enzymatic reaction can be schematized in two steps. First, we have the formation of the scaffold-enzyme complex,

which happens when the two proteins come within a distance of 1.5σ. This complex can then react, with a probability dictated by an assigned microscopic rate λ_p. For the sake of simplicity, dephosphorylation is implemented as a unimolecular reaction with rate λ_{dp}. To reflect the strong directional driving that characterizes both phosphorylation and dephosphorylation in cellular conditions, the corresponding reverse reactions are suppressed by a factor of 10^{-6}. The complete reaction scheme is illustrated in Fig. 1a.

Molecular simulations were performed using ReaDDy2 [34], which combines Brownian dynamics for particle motion with Monte Carlo–style steps to model chemical reactions. Each reaction is attempted at a rate λ and accepted with a Metropolis-like probability that depends on the change in potential energy associated with the particle transformation. This is crucial in phase separated systems, where the high substrate concentration leads to strong interaction energies. This procedure enforces the principle of local detailed balance (LDB) [27], ensuring thermodynamic consistency by adjusting transition probabilities according to the local environment. Specifically, the probability of a single reaction event is reduced if it would increase the local potential energy. While each reaction obeys LDB, kinase localization introduces an asymmetry between the two reaction pathways, breaking global detailed balance and driving the system into a non-equilibrium steady state.

Condensate assembly depends on phosphorylation balance

To investigate the interplay between chemical reactions and condensation, we performed phase coexistence simulations using the *slab method*[23, 35, 36], in which the system is confined to an elongated box with periodic boundary conditions. This setup, illustrated in Fig. 1b, enables accurate sampling of the dilute and condensed phases as well as the interface, while reducing finite-size effects.

In our reactive system, phase equilibrium depends on the competition between phosphorylation and dephosphorylation processes. We therefore explore the system behavior by varying the phosphorylation microscopic rate λ_p, keeping the dephosphorylation rate fixed at $\lambda_{dp} = 0.005\,\tau^{-1}$. We note that the results presented here are valid for a wide range of λ_p and λ_{dp} values, as better detailed in the SI (Fig. S3b). For this set of simulations, we fixed $\varepsilon_P = 0.3$, so that phosphorylated proteins are effectively soluble. After a transient, the system reaches a steady state for all values of λ_p, with higher values leading to a larger fraction of phosphorylated proteins N_P (Fig. S4a).

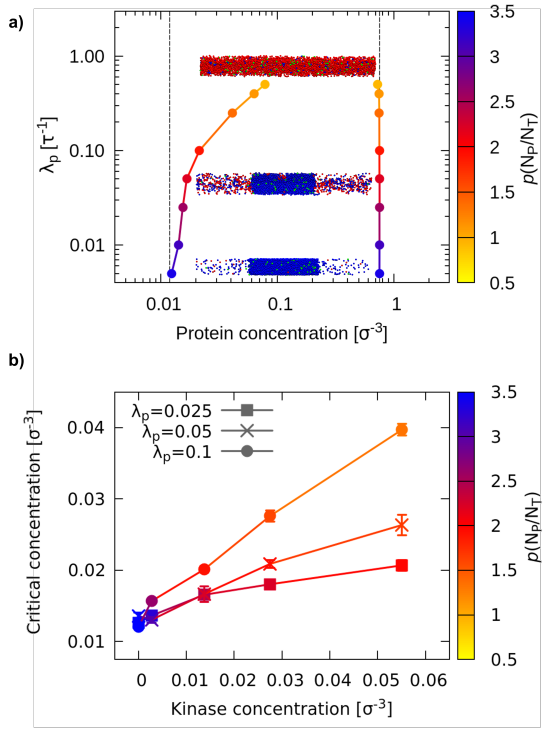

Figure 2: *Phase separation depends on reaction imbalance and enzyme concentration.* a) Phase diagram as a function of λ_p at fixed kinase concentration. For each value of λ_p, the two points represent the total protein concentration in the dilute and condensed phases, respectively. Each point is shaded to show the ratio of P particles (N_P) over the total (N_T) at steady state, following the scale on the left. The dashed bars represent the dilute and condensed phase concentrations at equilibrium. The snapshots illustrate different product concentrations P at different λ_p points and how they correlate with phase separation. b) Saturation concentration as a function of kinase concentration, for three fixed values of λ_p .

We characterize the spatial organization in the resulting stationary states by constructing a phase diagram as a function of λ_p using dilute and condensed phase concentration of all proteins in the system (Fig. 2a). As the reaction cycle becomes more biased toward phosphorylation, the coexistence region progressively narrows: the dilute-phase concentration rises with λ_p, i.e., pushing the reaction balance towards phosphorylation. At the same time, the condensed-phase concentration remains largely unchanged. At $\lambda_p \geq 1.0\,\tau^{-1}$ the condensate dissolves completely, and the system becomes homogeneous. This is due to the compositional effect of increasing λ_p: as more scaffold proteins are phosphorylated,

they become more soluble and are depleted from the condensed phase, resulting in its gradual shrinkage. Since the total number of proteins is fixed, the increase in the scaffold protein number N_P leads to an enrichment of the dilute phase. The resulting phase behavior closely matches that of a passive, non-reactive system with fixed composition, where the fraction N_P/N_T (where N_T is the total protein number) directly controls phase separation (Fig. S4b).

We then explore how the phase behavior depends on the concentration of kinases ρ_K. Figure 2b shows the saturation concentration (*i.e.* the dilute-phase boundary) as a function of ρ_K, revealing a linear dependence that mirrors experimental observations for the DYRK3 kinase [9]. Consistent with the trend observed when varying λ_p, this behavior reflects the fact that increasing the number of kinases raises the steady-state fraction of phosphorylated proteins N_P/N_T, which, in turn, governs the degree of condensation. Overall, these results show that enzymatic activity controls condensate assembly primarily by tuning the steady-state fraction of phase-separating proteins, effectively acting as a non-equilibrium control parameter for phase coexistence.

Modification strength maximizes regulatory efficiency at the solubility threshold

PTMs can alter the energy of intermolecular interactions to various degrees, especially when considering the possibility of multi-site modifications [37, 38, 39]. A recent study suggests that multisite phosphorylation provides a tunable mechanism for controlling protein-protein interaction strength: only after a critical number of sites have been phosphorylated, the homotypic interaction is weakened enough for the proteins to leave the condensed phase [28]. Here, we investigate how such variability in PTM-induced interaction modifications affects the steady-state properties of phase separation. We model this feature of a PTM driven system by introducing the parameter

$$\Delta\varepsilon = \varepsilon_N - \varepsilon_P = 1 - \varepsilon_P$$

which quantifies the change in intermolecular interaction energy upon enzymatic modification. We refer to this property as the *modification strength*. An increase in $\Delta\varepsilon$ corresponds to a stronger phosphorylation effect, which disfavors the interaction between phosphorylated proteins and the rest of the system.

Interestingly, the simulations reveal a non-monotonic relationship between the phase separation propensity of the system and the modification strength, as illustrated by the snapshots in Fig. 3a.

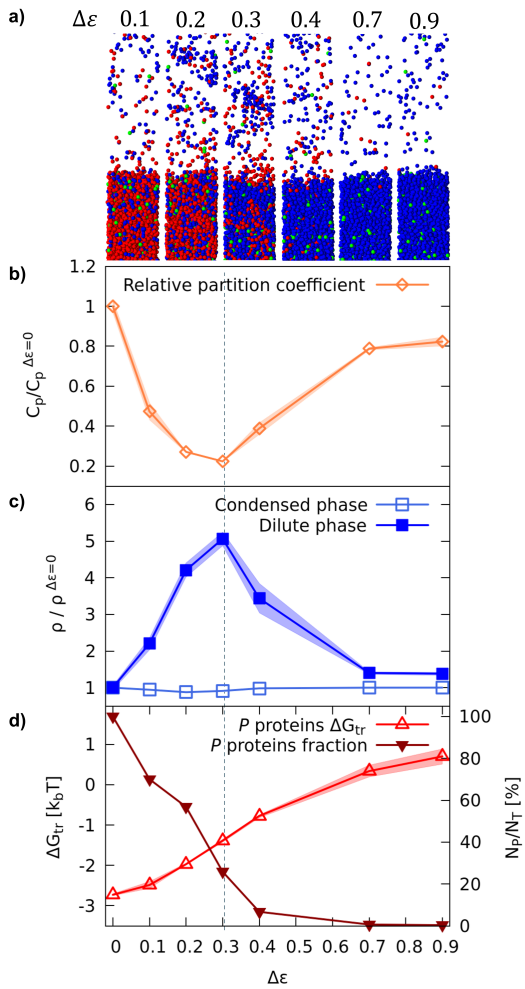

Figure 3: *Phase behavior depends on the intensity of interaction modifications induced by phosphorylation.* a) Snapshots from the simulations showing the phase coexistence. b) Partition coefficient of all proteins as a function of $\Delta\varepsilon$, normalized with respect to its value at $\Delta\varepsilon = 0$. Lower C_p means that proteins prefer the dilute phase, which increases the critical concentration. The grey line represent the critical $\Delta\varepsilon$ over which P proteins are no longer able to phase separate on their own. c) Protein concentration of the dilute phase (full squares) and dilute phase (empty square), normalized with respect to their value at $\Delta\varepsilon = 0$. d) Free energy of transfer of P proteins compared to their fraction as a function of $\Delta\varepsilon$. Higher transfer free energies mean that proteins prefer to partition in the dilute phase (see Methods). The point at $\Delta\varepsilon = 0$ is taken from the simulations with no reactions and only scaffold proteins. All data presented in this figure was obtained from simulations at $\lambda_p = 0.05$.

We quantify the dependence of condensation on the modification strength $\Delta\varepsilon$ by tracking the total partition coefficient C_p of the system (Fig. 3b). C_p is the ratio of the protein concentrations in the condensed (ρ_{dens}) and dilute phase (ρ_{dil}): higher values of C_p mean that proteins favor partitioning inside the condensate. For small modification strengths ($\Delta\varepsilon \leq 0.3$), increasing $\Delta\varepsilon$ leads to a decrease in C_p, i.e. phase separation becomes less favorable. This trend is coherent with our expectation of enhanced phase separation regulation, as higher $\Delta\varepsilon$ values favor the solubilization of P in the dilute phase. When increasing $\Delta\varepsilon$ beyond 0.3, however, C_p increases: yet again, phase separation tends to be favored. Hence, C_p has a minimum at $\Delta\varepsilon \approx 0.3$, which means that the system is at maximum solubility. The snapshots visually highlight this effect, showing a significantly denser dilute phase for the simulation at $\Delta\varepsilon = 0.3$. Decoupling the effect on C_p of the concentrations of the two phases (Fig. 3c) we observe that the non-monotonic behavior is mostly due to the variation in dilute concentration, with the condensed phase concentration remaining mostly constant. The complete phase diagrams at different values of $\Delta\varepsilon$ (Fig. S5b) further show that the system has the narrowest phase separation region at $\Delta\varepsilon \approx 0.3$. Notably, this value corresponds to the interaction energy below which P proteins are unable to phase separate on their own. Furthermore, this non-monotonic behavior is more pronounced for higher values of the phosphorylation rate, λ_p (Fig. S5a).

To rationalize this behavior, we recall that phase separation is primarily determined by the steady-state P protein fraction, as established in the previous section. In Fig. 3d, we report the dependence of the P protein fraction (N_P/N_T) and the transfer free energy (ΔG_trans) of P proteins between the two phases on $\Delta\varepsilon$. As expected, ΔG_trans increases with $\Delta\varepsilon$, indicating that P proteins increasingly disperse in the dilute phase. Concurrently, however, the fraction of P proteins decreases drastically. This reduction in P fraction compensates for their increased solubility, explaining why the condensed phase is stabilized at high $\Delta\varepsilon$: although individual P proteins are more soluble, their lower abundance diminishes their overall disruptive effect on phase separation. Furthermore, the height of the P fraction curve increases with $\lambda_\mathrm{p}/\lambda_\mathrm{dp}$, which explains the higher dilute concentrations at higher ratios, as ΔG_trans itself shows no such dependency (Fig. S5c).

The drop in P protein fraction arises because stronger phosphorylation imposes a higher energetic penalty for the phosphorylation reaction. This ultimately leads to a lower phosphorylation rate, particularly within the densely packed condensed phase. For $\Delta\varepsilon \leq 0.3$, the P fraction remains high, but their attraction to unmodified N proteins is still sufficient to retain them in the condensed phase, as seen in the two leftmost snapshots of Fig. 3. Regulation is thus most effective near the solubility threshold of P proteins. At this point the modification is sufficient to induce their dispersion from the condensate, yet their concentration remains high enough to significantly hinder phase separation. More generally, these findings define an optimal energetic regime for active control, in which post-translational modifications tune condensate stability by placing the system at the edge of phase separation.

Condensates interface is the nexus of chemical activity

So far, we have characterized the system behavior in terms of global observables, such as phase diagrams and average protein concentrations. We now explore local properties to better understand the interplay between chemical regulation and spatial organization, particularly at the interface.

We first examine the spatial distribution of phosphorylation and dephosphorylation reaction fluxes, calculated as the total amount of reaction per unit of time and surface across the *xy* plane (Fig. 4a). Remarkably, the phosphorylation flux exhibits a pronounced peak at the interface between the condensed and dilute phases. Notably, this spatial localization of chemical activity is not expected in models that assume homogeneous reaction rates, and instead emerges from the local modulation of reaction kinetics by the local environment. Inside the condensate, the high concentrations of scaffold proteins (N) and kinases (K) favor frequent encounters between enzymes and substrates. Still, the dense environment also increases the energetic penalty for converting N to P, which reduces the effective reaction rate (Figure 4b top panel). This suppression is modulated by the phosphorylation strength $\Delta\varepsilon$: stronger modifications incur a larger energetic penalty, further reducing phosphorylation rates in the condensed phase (Fig. S6a), consistent with the non-monotonic behavior of phase stability described in the previous section. At the interface, N and K concentrations remain relatively high, but scaffold proteins experience fewer stabilizing interactions, lowering the energetic cost of phosphorylation. This leads to enhanced reaction activity specifically at the boundary between phases. In contrast to phosphorylation, the dephosphorylation flux closely follows the spatial distribution of P proteins. Since converting P to N generally leads to more favorable interactions, the reaction does not incur an energetic penalty. As a result, its effective rate is largely insensitive to the local environment, and the flux is primarily shaped by substrate availability.

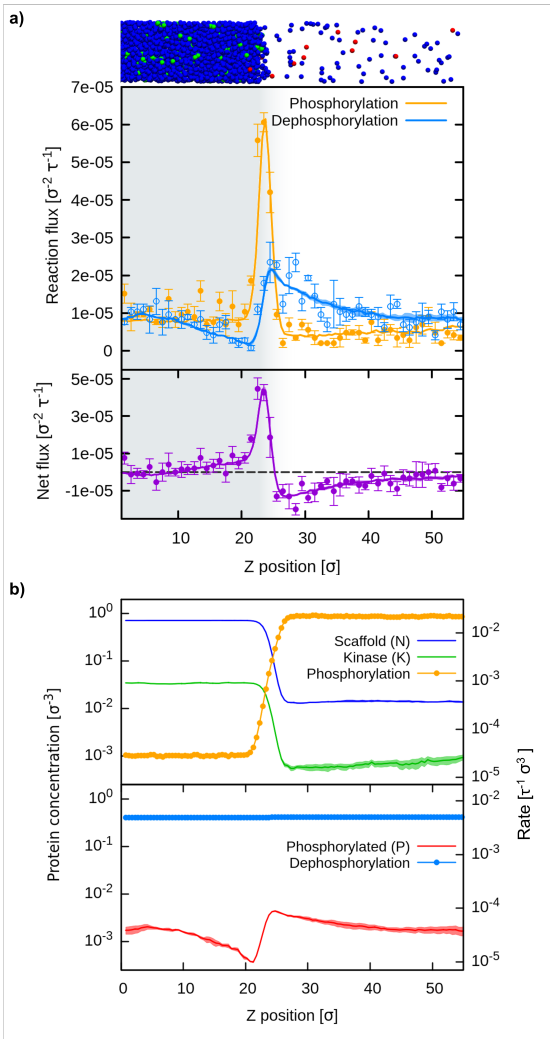

Figure 4: *Phosphorylation accumulation at the condensate's interface.* In this figure, we represent different quantities as a function of the distance from the center of the condensed phase. Data from the simulations at $\lambda_p = 0.05\,\tau^{-1}$, $\varepsilon_P = 0.3$. a) Rate flux of the two reactions. Fluxes were quantified by direct reaction counting (dots), and reaction activity recomputation (line, see Methods). The bottom plot shows the net particle flux at the interface (positive means more P proteins produced). The shaded area indicates the extension of the condensed phase. b) Comparison between protein concentration and microscopic reaction rates of phosphorylation (top panel) and dephosphorylation (bottom panel). Protein concentrations are plotted on the left y axis, while the microscopic rate is plotted on the right y axis.

The phosphorylation and dephosphorylation fluxes do not compensate near the phase boundary, resulting in a net production of phosphorylated proteins (P) within the condensed phase and of non-phosphorylated proteins (N) in the dilute phase (Fig. 4a, bottom panel). This asymmetric reaction distribution gives rise to a localized and directional flux across the interface with P proteins continuously exiting the condensate while N proteins are replenished from the dilute phase. Such sustained directional fluxes are a hallmark of non-equilibrium systems driven by active processes. To assess the impact of the interface also under equilibrium conditions, we simulate a version of the model with no explicit enzymes in which both reactions are reversible and unimolecular. As expected, the system shows no net chemical flux. Nonetheless, both reactions display pronounced peaks near the interface, showing that spatial variations in density and interactions can concentrate reaction activity even in the absence of energy input (Fig. S6b).

To corroborate the potential role of the interface as a localized catalytic environment, the question arises whether in real-world biomolecular condensates the interfacial region is large enough that its relative weight can significantly impact the overall chemical activity. Indeed, assuming that the width of the interface only depends on the interaction of the condensate components and not on its size, the ratio of the interface and total volumes will decrease with the condensate radius. Hence, we perform slab simulations of phase separating proteins FUS and NDDX4 to measured the spatial extension of the interface, based on the intermolecular energy profile (see Methods section). Assuming a fixed interface width $l = 14\,\text{nm}$, as measured in these higher resolution simulations (Fig. 5a), we can then calculate the weight of the interface chemical activity (Fig. 5b). This percentage can be quite high ($> 20\%$) even for spherical condensates larger than $1\,\mu\text{m}$. Since the size of typical cellular condensates rarely exceeds the $2\,\mu\text{m}$ diameter, we note that the weight of the interface flux is significant even for very large condensates. Considering that many FUS- or NDDX4-based condensates are indeed smaller than $1\,\mu\text{m}$, and often exhibit non-spherical shapes, we deem ours a conservative estimate of the impact of the interfacial catalytic enhancement. Altogether, these results identify the condensate interface as an emergent reactive hub, whose contribution to chemical activity remains significant even at biologically relevant length scales.

Discussion

In this study, we develop and use an ultra-coarse-grained molecular model to investigate the phase behavior and reactive properties of biomolecular condensates stabilized by enzymatic modifications. Using particle-based reactive simulations

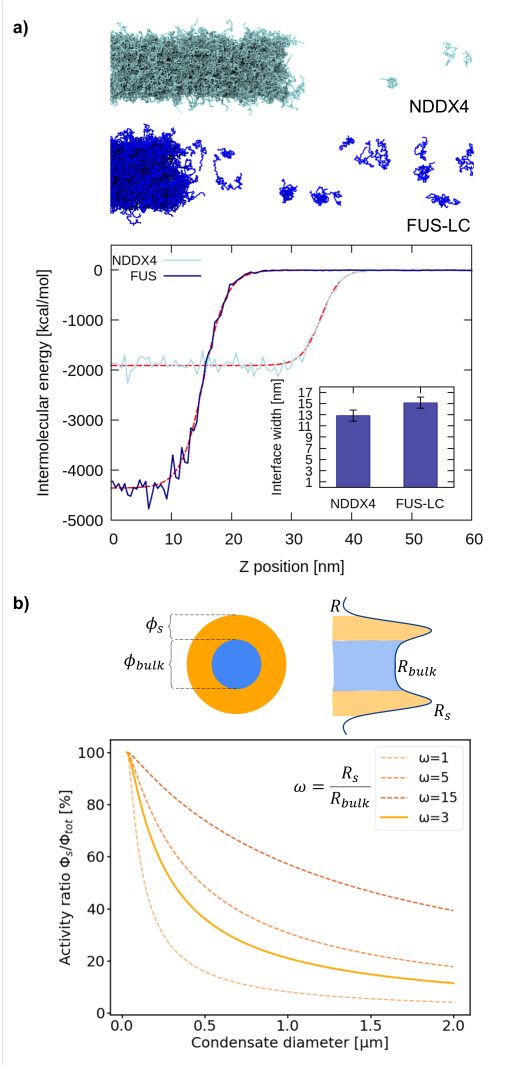

Figure 5: *The interface effect is relevant for real-world condensates.* a) Intermolecular energy as a function of the distance from slab center, from the CALVADOS simulations of NDDX4 and FUS-LC proteins. The dashed red lines represent the fitted data, through which we extracted the interfacial width shown in the inset (see Methods section). On top, snapshots of the phase coexistence simulations of the two proteins. b) Estimate of the relative weight of the interfacial activity in a spherical condensate, as a function of the diameter. In the sketch, we illustrate the involved quantities: the total amount of reactions per time Φ_S and Φ_{bulk} are obtained by multiplying the average rates R_S and R_{bulk} by the respective volumes. The ratio Φ_S/Φ_{tot} is plotted at fixed interfacial width $l = 14\,\text{nm}$ and at different values of ω. These values have the same order of magnitude of the ratio R_S/R_{bulk} measure in our simulations (see Methods).

with reaction rules that respect thermodynamic constraints, we show how enzymatic activity modulates the nonequilibrium phase behavior of the system: as the balance shifts toward phosphorylation, either through increased kinase rate or concentration, the condensate phase shrinks and ultimately dissolves [19]. In our model, enzymatic regulation plays a role analogous to temperature in upper critical solution temperature (UCST) systems, acting as a control parameter for condensate stability. The novelty of our system is the nonequilibrium drive intrinsic in the phosphorylation/dephosphorylation reaction scheme. This mechanism leads to a different principle for phase separation: the balance between the two reaction paths controls the concentration of phase-separating material. To our knowledge, our results provide the first phase diagram established for such a nonequilibrium regime.

A crucial aspect of our model is the application of the local detailed balance reaction scheme, which dynamically tunes reaction rates by taking into account the surrounding environment, thereby granting thermodynamic coherence to the system. A first, direct consequence of this feature is the observed reduction in phosphorylation rate inside the condensed phase. Previous experimental studies have highlighted how condensates are used by the cell to inhibit biochemical reactions, for instance to prevent decay of unstable proteins in case of external stress [40], or to regulate enzyme activity [41].

This mechanism leads to a non-monotonic dependence of the regulatory efficacy on the strength of the protein scaffold modification upon reaction. Indeed, enzymatic regulation improves with modification strength only if the modified proteins are still sticky enough to phase separate on their own. After that threshold, modification rates inside the condensed phase fall due to the unfavorable environment, leading to a decrease of the regulatory efficacy. In other words, our data indicate that phase separation is most sensitive to post-translational modifications that are just strong enough to prevent modified proteins from remaining in the condensed phase. This means that there is an optimal value of PTM strength that, if changed even slightly, leads to either reduced energetic efficiency or to uncontrollable phase separation.

The observation that minimal modification strength leads to maximum efficiency is coherent with the known principle by which proteins have evolved to exist at the edge of instability [42, 43]. We can predict this property withoutany assumption on the biological or molecular nature of the modification, but solely taking into account the enthalpic environment of the reactions.

Another feature directly caused by the LDB re-

action scheme is the concentration of material and chemical activity at the interface of the condensed phase. In particular, our simulations show a peak of phosphorylation activity at the interface, which is due to the more favorable environment. In our system phosphorylation is favored, by design, inside the condensate, coherently with experimental and theoretical indications [28, 33, 19]. Considering this interface effect, however, with reaction fluxes multiplied up to 5-fold, we predict that a significant portion of activity will happen on condensate's surfaces. Previous studies [19, 44] considered that a positive phosphorylation flux inside the condensate would suppress Ostwald ripening, which scales as R, thanks to its volumetric (R^3) scaling. We note that even if all regulation is concentrated at the interface, the flux would scale as R^2, which is still sufficient to balance condensate shrinking.

The importance of the interface effect is not limited to condensate regulation, but to any kind of biochemical activity, both enzymatic and non-enzymatic (Fig. S6), for which condensates are known catalytic platforms [43]. Experimental evidence showing enhanced rate in smaller enzymatic condensates [45] suggests that reaction rates scale with surface and not volume, indicating enhanced enzymatic activity at the interface. The phosphorylation peak, moreover, leads to P protein accumulation at the interface, which could be seen as an example of some features observed experimentally in chemically driven steady state condensates, such as core-shell substructuring [10, 46]. Hence, such an interface feature is to be added to the list of potential mechanisms by which phase separation regulates biochemical activity, along with crowding, and localization effects [47].

Interface structuring as an effect of the condensate crowded environment on reaction rates is a novel result on a problem, that of chemical activity at the condensed phase interface, the exploration of which started only recently [48, 49, 50] .

In summary, our simulations reveal key features of chemically regulated cellular condensates, with minimal assumptions on the biological nature of the involved proteins. We show that enforcing local thermodynamic consistency is crucial for a realistic picture of the system's steady state, due to the crowded nature of protein assemblies, even in an nonequilibrium scenario. Applying this measure to a model that allows sampling of the steady state, we identify an optimal range for intermolecular interaction modification and highlight the central role of the interface. While the present model is minimal, the mechanisms identified rely only on generic thermodynamic constraints and enzymatic driving, defining principles broadly relevant for chemically regulated biomolecular condensates. Building on this generality, the versatility of the model provides a foundation to explore diverse systems by incorporating additional components or more complex reaction schemes.

Methods

1-bead-per-molecule simulations To simulate the steady state of our phase separating ultra-CG model, we relied on the ReaDDy2 software package [34]. The time evolution of particle diffusion was simulated following the overdamped Langevin equation, with the diffusion coefficient D for all molecules set to unity. These simulations were run with a time-step $\tau = 2 \times 10^{-4}\,\hat{\mathrm{t}}$, with $\hat{t} = \sigma^2 D^{-1}$ being the time unit in our reduced system, as better detailed in section Extended Methods of the SI. Particles interacted through a truncated and shifted Lennard-Jones pair potential, with the truncation set at the standard value of 2.5σ. The reactions were handled by the LDB algorithm included in ReaDDy [27]. At each time step and for each reaction, all reactive particles would attempt a reaction step with probability $P = 1 - e^{-\lambda\tau}$, with λ the microscopic rate for that reaction. After that, the reaction was accepted or rejected with a Monte Carlo check of the system's potential energy. We choose microscopic reaction rates of the driven reactions in the range of $0.005\,\hat{\mathrm{t}}$ to $2.0\,\hat{\mathrm{t}}$, which allowed for proper sampling of the phase separation steady-state. A more thorough discussion on the connection between microscopic rates in our model and real-world enzymatic systems can be found in section of the SI.

All phase coexistence simulations were performed in triclinic boxes with periodic boundary conditions of size $x = y = 11\,\sigma$ and $z = 120\,\sigma$, with the condensed phase spanning the xy plane. The boxes were initialized with the particles arranged in a cubic lattice with minimal distance σ, placed in the center of the box to obtain a slab configuration. Each simulation contained 4400 particles. We let the simulations run until both the number of particles and the concentration of dilute and condensed phases reached a steady state for at least $2000\,\hat{\mathrm{t}}$. Since equilibration times varied depending on initial configuration, composition, and set of parameters, not all simulations had the same run-time, but all ranged between 3000 and $5000\,\hat{\mathrm{t}}$. All data, including system trajectory, were saved with a frequency of $0.4\,\hat{\mathrm{t}}$ ($2000\,\tau$). We replicated each simulation three times, and steady-state quantities are measured as the average over these three replicas.

For the phase diagram in λ_{p}, we explored λ_{p} values by varying the phosphorylation rate λ_{p} while

keeping $\lambda_{\text{dp}} = 0.005\,\tau^{-1}$, for each value of $\Delta\varepsilon$. We fixed the kinase concentration at$\rho_K = 0.014\,\sigma^{-3}$, low enough to prevent phase separation by kinases themselves.

Reactions The chemical reactions included in the model are the kinase-mediated phosphorylation and a spontaneous dephosphorylation (we implicitly consider the phosphatase to be diffuse in the system). These reactions are schematized below, with particles not explicitly included in the system written within round brackets

$$(ATP) + K + N \rightleftharpoons (ADP) + K + P \quad (1)$$
$$P \rightleftharpoons N + (Phosphate) \quad (2)$$

We label the forward reaction rates of equation 1, 2, i.e. reading the reactions from left to right, respectively R_1^f, R_2^f, while the backward rates R_1^b, R_2^b correspond to reading reactions 1, 2 from right to left.

Overall conversion rates $N \to P$ ($R_{N\to P}$) and $P \to N$ ($R_{P\to N}$) are thus defined as

$$R_{N\to P} = R_1^f + R_2^b \quad (3)$$
$$R_{P\to N} = R_2^f + R_1^b \quad (4)$$

In the dilute limit, reaction rates can be written as follows

$$R_1^f = k_1 \rho_N \rho_K \langle e^{-\beta\Delta U}\rangle \quad (5)$$
$$R_1^b = k_1 e^{-\beta\Delta\mu_1} \rho_P \rho_K \quad (6)$$
$$R_2^f = k_2 \rho_P \quad (7)$$
$$R_2^b = k_2 e^{-\beta\Delta\mu_2} \rho_N \langle e^{-\beta\Delta U}\rangle \quad (8)$$

where k_1 and k_2 are microscopic transition probabilities, β is the inverse of $k_B T$, ρ_i is the concentration of species i and $\langle e^{-\beta\Delta U}\rangle$ represents the ensemble average of the Boltzmann factor used in the LDB algorithm. Backwards rates are suppressed by a factor $e^{\beta\Delta\mu_i} \simeq 10^6$ with respect to their corresponding forward rates, which takes into account the chemical driving of implicit particles involved in reaction i. In our reaction scheme, $\Delta\mu_1 = \mu_{ATP} - \mu_{ADP}$ and $\Delta\mu_2 = \mu_{H_2O} - \mu_{Phos}$.

1-bead-per-residue simulations Slab simulations of FUS-LC and NDDX4 protein condensates were performed using the OpenMM package with the CALVADOS2 force field [51]. The simulations were produced using a Langevin integrator with time step 0.01 ps at a temperature of 300 K and a relaxation time of 100 ps. All simulations were carried out in two parts: an equilibration in the NPT ensemble to stabilize the condensed phase and a production run in the slab configuration in the NVT ensemble. Total simulated time in the production run was 10 µs.

Calculation of dilute and condensed phase concentrations In a slab simulation, properties like the concentration of particles can be plotted in a dome-like profile, as visible in Fig. 1a. To extract the concentrations of condensed and dilute phases from these configurations, we first computed the total density profiles, averaging over $100\hat{\tau}$ time windows and symmetrizing with respect to the center of the condensate, identified with the position of the center of mass of the system. Then, for each profile, we performed a fit based on an adapted hyperbolic tangent function, as proposed by Tesei et al. [52].

Calculation of the free energy of transfer To calculate the free energy of transfer, ΔG_{trans}, we exploited the results from the fit of the concentration with the hyperbolic tangent function to set the z position of the interfaces between the two phases. For each frame, we counted the number of protein molecules within the condensed phase, N_{in}, and the dilute phase, N_{out}. The partitioning coefficient was determined as the ratio of the respective number densities, $K_p = (\langle N_{\text{in}}\rangle/V_{\text{in}})/(\langle N_{\text{out}}\rangle/V_{\text{out}})$, where V_{in} and V_{out} are the volumes of the two phases. The free energy was then obtained from the relation $\Delta G_{\text{trans}} = -k_B T \ln K_p$.

Recomputation of expected local rates To calculate the local reaction rates without relying only on reaction counts, which are relatively low, we performed an indirect recomputation based on the trajectory. In each step of the saved trajectory, we looped over all reactive particles and measured the ΔU associated with the available reaction. From the ΔU, we could obtain the acceptance probability $a(\Delta U)$ and the reaction rate of that particle, and average their values over all particles in the same z bin and over time. Since the rates obtained through the recomputation are in good agreement with the direct reaction count and have relatively lower signal noise, we utilized those to illustrate other analyses throughout this study, including acceptance probability and ΔU.

Calculation of the interface flux percentage While the difference in intermolecular energy inside and outside the condensed phase varies significantly between condensates composed of the two proteins, the width of the interface is similar and measures around 14 nm (Fig. 5a). We estimate the relative weight of the reaction flux for a spherical condensate as a function of its radius, using this equation

$$\frac{\Phi_S}{\Phi_{tot}} = \frac{\omega V_S}{\omega V_S + V_{bulk}} \quad (9)$$

where Φ_S and Φ_{tot} are the total reaction fluxes from the interface and the whole condensate, $\omega = \frac{R_S}{R_{bulk}}$ is the ratio between the average reaction flux

in the interface region and bulk of the condensate, V_S the volume of the interface and V_{bulk} the volume of the bulk (see the sketch in Fig. 5b). From this equation, it is possible to express $\frac{\Phi_S}{\Phi_{tot}}$ as a function of the condensate radius and width of the interface shell.

References

[1] Yongdae Shin and Clifford P. Brangwynne. Liquid phase condensation in cell physiology and disease, 9 2017. ISSN 10959203. URL https://www.science.org/doi/10.1126/science.aaf4382.

[2] Clifford P. Brangwynne, Christian R. Eckmann, David S. Courson, Agata Rybarska, Carsten Hoege, Jöbin Gharakhani, Frank Jülicher, and Anthony A. Hyman. Germline P granules are liquid droplets that localize by controlled dissolution/condensation. *Science*, 324(5935): 1729–1732, 6 2009. ISSN 00368075. doi: 10.1126/SCIENCE.1172046/SUPPL{_}FILE/BRANGWYNNE.SOM.PDF. URL https://www.science.org/doi/10.1126/science.1172046.

[3] Benjamin R. Sabari, Alessandra Dall'Agnese, and Richard A. Young. Biomolecular Condensates in the Nucleus. *Trends in Biochemical Sciences*, 45(11):961–977, 11 2020. ISSN 09680004. doi: 10.1016/j.tibs.2020.06.007. URL https://linkinghub.elsevier.com/retrieve/pii/S0968000420301675.

[4] Amandine Molliex, Jamshid Temirov, Jihun Lee, Maura Coughlin, Anderson P. Kanagaraj, Hong Joo Kim, Tanja Mittag, and J. Paul Taylor. Phase Separation by Low Complexity Domains Promotes Stress Granule Assembly and Drives Pathological Fibrillization. *Cell*, 163 (1):123–133, 9 2015. ISSN 0092-8674. doi: 10.1016/J.CELL.2015.09.015.

[5] Pilong Li, Sudeep Banjade, Hui Chun Cheng, Soyeon Kim, Baoyu Chen, Liang Guo, Marc Llaguno, Javoris V. Hollingsworth, David S. King, Salman F. Banani, Paul S. Russo, Qiu Xing Jiang, B. Tracy Nixon, and Michael K. Rosen. Phase transitions in the assembly of multivalent signalling proteins. *Nature 2012 483:7389*, 483(7389):336–340, 3 2012. ISSN 1476-4687. doi: 10.1038/nature10879. URL https://www.nature.com/articles/nature10879.

[6] Salman F. Banani, Hyun O. Lee, Anthony A. Hyman, and Michael K. Rosen. Biomolecular condensates: organizers of cellular biochemistry. *Nature Reviews Molecular Cell Biology 2017 18:5*, 18(5):285–298, 2 2017. ISSN 1471-0080. doi: 10.1038/nrm.2017.7. URL https://www.nature.com/articles/nrm.2017.7.

[7] Anthony A. Hyman, Christoph A. Weber, and Frank Jülicher. Liquid-Liquid Phase Separation in Biology. *Annual Review of Cell and Developmental Biology*, 30(1): 39–58, 10 2014. ISSN 1081-0706. doi: 10.1146/annurev-cellbio-100913-013325. URL https://www.annualreviews.org/doi/10.1146/annurev-cellbio-100913-013325.

[8] Juan Manuel Valverde, Geronimo Dubra, Michael Phillips, Austin Haider, Carlos Elena-Real, Aurélie Fournet, Emile Alghoul, Dhanvantri Chahar, Nuria Andrés-Sanchez, Matteo Paloni, Pau Bernadó, Guido van Mierlo, Michiel Vermeulen, Henk van den Toorn, Albert J R Heck, Angelos Constantinou, Alessandro Barducci, Kingshuk Ghosh, Nathalie Sibille, Puck Knipscheer, Liliana Krasinska, Daniel Fisher, and Maarten Altelaar. A cyclin-dependent kinase-mediated phosphorylation switch of disordered protein condensation. *Nature Communications*, 14(1):6316, 10 2023. ISSN 2041-1723. doi: 10.1038/s41467-023-42049-0. URL https://www.nature.com/articles/s41467-023-42049-0.

[9] Arpan Kumar Rai, Jia Xuan Chen, Matthias Selbach, and Lucas Pelkmans. Kinase-controlled phase transition of membraneless organelles in mitosis. *Nature 2018 559:7713*, 559(7713):211–216, 7 2018. ISSN 1476-4687. doi: 10.1038/s41586-018-0279-8. URL https://www.nature.com/articles/s41586-018-0279-8.

[10] Alexander M. Bergmann, Jonathan Bauermann, Giacomo Bartolucci, Carsten Donau, Michele Stasi, Anna-Lena Holtmannspötter, Frank Jülicher, Christoph A. Weber, and Job Boekhoven. Liquid spherical shells are a non-equilibrium steady state of active droplets. *Nature Communications*, 14(1):6552, 10 2023. ISSN 2041-1723. doi: 10.1038/s41467-023-42344-w. URL https://www.nature.com/articles/s41467-023-42344-w.

[11] Maria Hondele, Stephanie Heinrich, Paolo De Los Rios, and Karsten Weis. Membraneless organelles: phasing out of equilibrium. *Emerging Topics in Life Sciences*, 4(3):343–354, 12 2020. ISSN 2397-8554. doi: 10.1042/ETLS20190190. URL https://portlandpress.com/emergtoplifesci/article/4/3/343/225959/Membraneless-organelles-phasing-out-of-equilibrium.

[12] Miriam Linsenmeier, Maria Hondele, Fulvio Grigolato, Eleonora Secchi, Karsten Weis, and Paolo Arosio. Dynamic arrest and aging of biomolecular condensates are modulated by low-complexity domains, RNA and biochemical activity. *Nature Communications*, 13(1): 3030, 5 2022. ISSN 2041-1723. doi: 10.1038/s41467-022-30521-2.

[13] Carsten Donau, Fabian Späth, Michele Stasi, Alexander M. Bergmann, and Job Boekhoven. Phase Transitions in Chemically Fueled, Multiphase Complex Coacervate Droplets. *Angewandte Chemie - International Edition*, 61 (46), 11 2022. ISSN 15213773. doi: 10.1002/anie.202211905.

[14] Sebastian Coupe and Nikta Fakhri. ATP-induced cross-linking of a biomolecular condensate. *Biophysical Journal*, 123(11):1356–1366, 6 2024. ISSN 15420086. doi: 10.1016/j.bpj.2023.07.013.

[15] Matthew Amato, June Ho Hwang, Manolo U. Rios, Nicole E. Familiari, Michael K. Rosen, and Jeffrey B. Woodruff. Phospho-regulated tuning of viscoelastic properties balances centrosome growth and strength. *bioRxiv*, page 2024.08.29.610374, 8 2024. doi: 10.1101/2024.08.29.610374. URL https://www.biorxiv.org/content/10.1101/2024.08.29.610374v1https://www.biorxiv.org/content/10.1101/2024.08.29.610374v1.abstract.

[16] Emery T. Usher, Martin J. Fossat, and Alex S. Holehouse. Phosphorylation of disordered proteins tunes local and global intramolecular interactions. *Biophysical Journal*, 123(23):4082–4096, 12 2024. ISSN 00063495. doi: 10.1016/j.bpj.2024.10.021. URL https://linkinghub.elsevier.com/retrieve/pii/S0006349524007094.

[17] David Zwicker, Rabea Seyboldt, Christoph A. Weber, Anthony A. Hyman, and Frank Jülicher. Growth and division of active droplets provides a model for protocells. *Nature Physics*, 13(4):408–413, 4 2017. ISSN 17452481. doi: 10.1038/NPHYS3984;SUBJMETA=530,639,747,766;KWRD=BIOLOGICAL+PHYSICS,STATISTICAL+PHYSICS. URL https://www-nature-com.insb.bib.cnrs.fr/articles/nphys3984.

[18] Jean David Wurtz and Chiu Fan Lee. Chemical-Reaction-Controlled Phase Separated Drops: Formation, Size Selection, and Coarsening. *Physical Review Letters*, 120(7), 2 2018. ISSN 10797114. doi: 10.1103/PhysRevLett.120.078102.

[19] Jan Kirschbaum and David Zwicker. Controlling biomolecular condensates via chemical reactions. *Journal of The Royal Society Interface*, 18(179):20210255, 6 2021. ISSN 1742-5662. doi: 10.1098/rsif.2021.0255. URL https://royalsocietypublishing.org/doi/10.1098/rsif.2021.0255.

[20] Noah Ziethen, Jan Kirschbaum, and David Zwicker. Nucleation of Chemically Active Droplets. *Physical Review Letters*, 130 (24):248201, 6 2023. ISSN 10797114. doi: 10.1103/PHYSREVLETT.130.248201/FIGURES/3/MEDIUM. URL https://journals.aps.org/prl/abstract/10.1103/PhysRevLett.130.248201.

[21] Alexandra Shelest, Hugo Le Roy, Daniel M. Busiello, and Paolo De Los Rios. Phase boundaries promote chemical reactions through localized fluxes. *Journal of Chemical Physics*, 162(2):24112, 1 2025. ISSN 10897690. doi: 10.1063/5.0242782/3329661. URL /aip/jcp/article/162/2/024112/3329661/Phase-boundaries-promote-chemical-reactions.

[22] Matteo Paloni, Rémy Bailly, Luca Ciandrini, and Alessandro Barducci. Unraveling Molecular Interactions in Liquid–Liquid Phase Separation of Disordered Proteins by Atomistic Simulations. *The Journal of Physical Chemistry B*, 124(41):9009–9016, 10 2020. ISSN 1520-6106. doi: 10.1021/acs.jpcb.0c06288. URL https://doi.org/10.1021/acs.jpcb.0c06288.

[23] Gregory L Dignon, Wenwei Zheng, Robert B Best, Young C Kim, and Jeetain Mittal. Relation between single-molecule properties and phase behavior of intrinsically disordered proteins. *Proceedings of the National Academy of Sciences*, 115(40):9929–9934, 10 2018. doi: 10.1073/pnas.1804177115. URL https://www.pnas.org/doi/abs/10.1073/pnas.1804177115.

[24] Nicola Galvanetto, Miloš T Ivanović, Aritra Chowdhury, Andrea Sottini, Mark Nüesch, Daniel Nettels, Robert Best, and Benjamin Schuler. Ultrafast molecular dynamics observed within a dense protein condensate, 12 2022. URL https://www.biorxiv.org/content/10.1101/2022.12.12.520135v1.

[25] Adiran Garaizar, Jorge R Espinosa, Jerelle A Joseph, Georg Krainer, Yi Shen, Tuomas P J Knowles, and Rosana Collepardo-Guevara. Aging can transform single-component protein condensates into multiphase architectures. *Proceedings of the National Academy of Sciences*, 119(26):e2119800119, 6 2022. doi: 10.1073/pnas.2119800119. URL https://www.pnas.org/doi/full/10.1073/pnas.2119800119.

[26] Jacques Fries, Javier Diaz, Marie Jardat, Ignacio Pagonabarraga, Pierre Illien, and Vincent Dahirel. Active droplets controlled by enzymatic reactions. 11 2024. URL http://arxiv.org/abs/2411.11696.

[27] Christoph Fröhner and Frank Noé. Reversible Interacting-Particle Reaction Dynamics. *Journal of Physical Chemistry B*, 122(49):11240–11250, 12 2018. ISSN 15205207. doi: 10.1021/ACS.JPCB.8B06981/ASSET/IMAGES/MEDIUM/JP-2018-06981V{_}M053.GIF. URL https://pubs.acs.org/doi/full/10.1021/acs.jpcb.8b06981.

[28] Emanuele Zippo, Dorothee Dormann, Thomas Speck, and Lukas S. Stelzl. Molecular simulations of enzymatic phosphorylation of disordered proteins and their condensates. *Nature Communications 2025 16:1*, 16 (1):1–16, 5 2025. ISSN 2041-1723. doi: 10.1038/S41467-025-59676-4. URL https://www-nature-com.insb.bib.cnrs.fr/articles/s41467-025-59676-4.

[29] Anastasia C Murthy, Gregory L Dignon, Yelena Kan, Gül H Zerze, Sapun H Parekh, Jeetain Mittal, and Nicolas L Fawzi. Molecular interactions underlying liquid-liquid phase separation of the FUS low-complexity domain. *Nature Structural & Molecular Biology*, 26 (7):637–648, 2 2019. ISSN 1545-9985. doi: 10.1038/s41594-019-0250-x. URL https://doi.org/10.1038/s41594-019-0250-x.

[30] Jacob P. Brady, Patrick J. Farber, Ashok Sekhar, Yi-Hsuan Lin, Rui Huang, Alaji Bah, Timothy J. Nott, Hue Sun Chan, Andrew J. Baldwin, Julie D. Forman-Kay, and Lewis E. Kay. Structural and hydrodynamic properties of an intrinsically disordered region of a germ cell-specific protein on phase separation. *Proceedings of the National Academy of Sciences*, 114(39), 9 2017. ISSN 0027-8424. doi: 10.1073/pnas.1706197114. URL https://pnas.org/doi/full/10.1073/pnas.1706197114.

[31] Ming-Tzo Wei, Shana Elbaum-Garfinkle, Alex S Holehouse, Carlos Chih-Hsiung Chen, Marina Feric, Craig B Arnold, Rodney D Priestley, Rohit V Pappu, and Clifford P Brangwynne. Phase behaviour of disordered proteins underlying low density and high permeability of liquid organelles. *Nature Chemistry*, 9(11):1118–1125, 2 2017. ISSN 1755-4349. doi: 10.1038/nchem.2803. URL https://doi.org/10.1038/nchem.2803.

[32] Wei Shi and J. Karl Johnson. Histogram reweighting and finite-size scaling study of the Lennard–Jones fluids. *Fluid Phase Equilibria*, 187-188:171–191, 9 2001. ISSN 0378-3812. doi: 10.1016/S0378-3812(01)00534-9. URL https://www.sciencedirect.com/science/article/pii/S0378381201005349#SEC8.

[33] William M. Aumiller and Christine D. Keating. Phosphorylation-mediated RNA/peptide complex coacervation as a model for intracellular liquid organelles. *Nature Chemistry 2015 8:2*, 8(2):129–137, 12 2015. ISSN 1755-4349. doi: 10.1038/nchem.2414. URL https://www.nature.com/articles/nchem.2414.

[34] Moritz Hoffmann, Christoph Fröhner, and Frank Noé. ReaDDy 2: Fast and flexible software framework for interacting-particle reaction dynamics. *PLOS Computational Biology*, 15(2):e1006830, 2 2019. ISSN 1553-7358. doi: 10.1371/journal.pcbi.1006830. URL https://dx.plos.org/10.1371/journal.pcbi.1006830.

[35] Gregory L. Dignon, Wenwei Zheng, and Jeetain Mittal. Simulation methods for liquid–liquid phase separation of disordered proteins. *Current Opinion in Chemical Engineering*, 23:92–98, 3 2019. ISSN 2211-3398. doi: 10.1016/J.COCHE.2019.03.004. URL https://www.sciencedirect.com/science/article/abs/pii/S2211339818300807.

[36] Kevin S. Silmore, Michael P. Howard, and Athanassios Z. Panagiotopoulos. Vapour–liquid phase equilibrium and surface tension of fully flexible Lennard–Jones chains. *Molecular Physics*, 115(3):320–327, 2 2017. ISSN 0026-8976. doi: 10.1080/00268976.2016.1262075.

[37] Mario Hofweber and Dorothee Dormann. Friend or foe-Post-translational modifications as regulators of phase separation and RNP granule dynamics. *Journal of Biological Chemistry*, 294(18):7137–7150, 5 2019. ISSN 1083351X. doi: 10.1074/JBC.TM118.001189/ASSET/B1D0AABF-E79B-4723-8C26-9493F72C8B24/MAIN.ASSETS/GR3.JPG. URL https://www.jbc.org/action/showFullText?pii=S0021925820367934https://www.jbc.org/action/showAbstract?pii=S0021925820367934https://www.jbc.org/article/S0021-9258(20)36793-4/abstract.

[38] Srivastav Ranganathan, Pouria Dasmeh, Seth Furniss, and Eugene Shakhnovich. Phosphorylation sites are evolutionary checkpoints against liquid-solid transition in protein condensates. *Proceedings of the National Academy of Sciences of the United States of America*, 120(20): e2215828120, 5 2023. ISSN 10916490. doi: 10.1073/PNAS.2215828120/SUPPL{_}FILE/PNAS.2215828120.SAPP.PDF. URL https://www.pnas.org/doi/abs/10.1073/pnas.2215828120.

[39] Mingwei Li, Guanglin Chen, and Zhiyong Zhang. Modeling the effects of phosphorylation on phase separation of the FUS low-complexity domain. *Biophysical Journal*, 122 (13):2636–2645, 7 2023. ISSN 15420086. doi: 10.1016/J.BPJ.2023.05.018/ATTACHMENT/2B3AAF15-4875-4CF4-A6A5-2BCC96B5D247/MMC2.PDF. URL https://www.cell.com/action/showFullText?pii=S0006349523003302https://www.cell.com/action/showAbstract?pii=S0006349523003302https://www.cell.com/biophysj/abstract/S0006-3495(23)00330-2.

[40] Yi Zhang, Geeta J. Narlikar, and Tatiana G. Kutateladze. Enzymatic Reactions inside Biological Condensates. *Journal of Molecular Biology*, 433(12):166624, 6 2021. ISSN 00222836. doi: 10.1016/j.jmb.2020.08.009.

[41] Manoël Prouteau, Ambroise Desfosses, Christian Sieben, Clélia Bourgoint, Nour Lydia Mozaffari, Davide Demurtas, Alok K. Mitra, Paul Guichard, Suliana Manley, and Robbie Loewith. TORC1 organized in inhibited domains (TOROIDs) regulate TORC1 activity. *Nature 2017 550:7675*, 550(7675):265–269, 10 2017. ISSN 1476-4687. doi: 10.1038/NATURE24021. URL https://www-nature-com.insb.bib.cnrs.fr/articles/nature24021.

[42] Hector Garcia-Seisdedos, Charly Empereur-Mot, Nadav Elad, and Emmanuel D. Levy. Proteins evolve on the edge of supramolecular self-assembly. *Nature 2017 548:7666*, 548(7666):244–247, 8 2017. ISSN 1476-4687. doi: 10.1038/NATURE23320. URL https://www-nature-com.insb.bib.cnrs.fr/articles/nature23320.

[43] Ying Zhang, Boguslaw Stec, and Adam Godzik. Between Order and Disorder in Protein Structures: Analysis of "Dual Personality" Fragments in Proteins. *Structure*, 15(9):1141–1147, 9 2007. ISSN 09692126. doi: 10.1016/j.str.2007.07.012. URL https://www.cell.com/action/showFullText?pii=S0969212607002857https://www.cell.com/action/showAbstract?pii=S0969212607002857https://www.cell.com/structure/abstract/S0969-2126(07)00285-7.

[44] Johannes Söding, David Zwicker, Salma Sohrabi-Jahromi, Marc Boehning, and Jan Kirschbaum. Mechanisms for Active Regulation of Biomolecular Condensates, 1 2020. ISSN 18793088. URL http://www.cell.com/article/S0962892419301795/fulltexthttp://www.cell.com/article/S0962892419301795/abstracthttps://www.cell.com/trends/cell-biology/abstract/S0962-8924(19)30179-5.

[45] Marcos Gil-Garcia, Ana I. Benítez-Mateos, Marcell Papp, Florence Stoffel, Chiara Morelli, Karl Normak, Katarzyna Makasewicz, Lenka Faltova, Francesca Paradisi, and Paolo Arosio. Local environment in biomolecular condensates modulates enzymatic activity across length scales. *Nature Communications 2024 15:1*, 15(1):1–11, 4 2024. ISSN 2041-1723. doi: 10.1038/s41467-024-47435-w. URL https://www.nature.com/articles/s41467-024-47435-w.

[46] Saumya Jain, Joshua R. Wheeler, Robert W. Walters, Anurag Agrawal, Anthony Barsic, and Roy Parker. ATPase-Modulated Stress Granules Contain a Diverse Proteome and Substructure. *Cell*, 164(3):487–498, 1 2016. ISSN 10974172. doi: 10.1016/J.CELL.

2015.12.038/ATTACHMENT/6B9EF878-A223-48E4-B440-AD629F8F27EF/MMC9.PDF. URL https://www.cell.com/action/showFullText?pii=S009286741501702Xhttps://www.cell.com/action/showAbstract?pii=S009286741501702Xhttps://www.cell.com/cell/abstract/S0092-8674(15)01702-X.

[47] Andrew S. Lyon, William B. Peeples, and Michael K. Rosen. A framework for understanding the functions of biomolecular condensates across scales. *Nature Reviews Molecular Cell Biology 2020 22:3*, 22(3): 215–235, 11 2020. ISSN 1471-0080. doi: 10.1038/S41580-020-00303-Z. URL https://www-nature-com.insb.bib.cnrs.fr/articles/s41580-020-00303-z.

[48] Christian Hoffmann, Gennadiy Murastov, Johannes Vincent Tromm, Jean Baptiste Moog, Muhammad Awais Aslam, Aleksandar Matkovic, and Dragomir Milovanovic. Electric Potential at the Interface of Membraneless Organelles Gauged by Graphene. *Nano Letters*, 23(23):10796–10801, 12 2023. ISSN 15306992. doi: 10.1021/ACS.NANOLETT.3C02915/ASSET/IMAGES/LARGE/NL3C02915{_}0004.JPEG. URL /doi/pdf/10.1021/acs.nanolett.3c02915?ref=article_openPDF.

[49] Nadia A. Erkamp, Mina Farag, Yuanxin Qiu, Daoyuan Qian, Tomas Sneideris, Tingting Wu, Timothy J. Welsh, Hannes Ausserwöger, Tommy J. Krug, Gaurav Chauhan, David A. Weitz, Matthew D. Lew, Tuomas P.J. Knowles, and Rohit V. Pappu. Differential interactions determine anisotropies at interfaces of RNA-based biomolecular condensates. *Nature Communications 2025 16:1*, 16(1):1–13, 4 2025. ISSN 2041-1723. doi: 10.1038/S41467-025-58736-Z. URL https://www-nature-com.insb.bib.cnrs.fr/articles/s41467-025-58736-z.

[50] Yongick Cho and William M. Jacobs. Interfacial effects determine nonequilibrium phase behaviors in chemically driven fluids. *Proceedings of the National Academy of Sciences*, 122(30), 7 2025. ISSN 0027-8424. doi: 10.1073/pnas.2501145122.

[51] Giulio Tesei, Thea K. Schulze, Ramon Crehuet, and Kresten Lindorff-Larsen. Accurate model of liquid-liquid phase behavior of intrinsically disordered proteins from optimization of single-chain properties. *Proceedings of the National Academy of Sciences of the United States of America*, 118(44): e2111696118, 11 2021. ISSN 10916490. doi: 10.1073/PNAS.2111696118/SUPPL{_}FILE/PNAS.2111696118.SAPP.PDF. URL https://www.pnas.org/doi/abs/10.1073/pnas.2111696118.

[52] Giulio Tesei and Kresten Lindorff-Larsen. Improved Predictions of Phase Behaviour of Intrinsically Disordered Proteins by Tuning the Interaction Range. 7 2022. doi: 10.1101/2022.07.09.499434. URL http://biorxiv.org/lookup/doi/10.1101/2022.07.09.499434.

[53] Ron Milo and Rob Phillips. *Cell Biology by the Numbers*. Garland Science, 12 2015. ISBN 9781317230694. doi: 10.1201/9780429258770.

[54] Mohit Kumar, Mario S. Mommer, and Victor Sourjik. Mobility of Cytoplasmic, Membrane, and DNA-Binding Proteins in Escherichia coli. *Biophysical Journal*, 98(4):552–559, 2 2010. ISSN 00063495. doi: 10.1016/j.bpj.2009.11.002.

[55] Carlos Salazar and Thomas Höfer. Kinetic models of phosphorylation cycles: A systematic approach using the rapid-equilibrium approximation for protein–protein interactions. *Biosystems*, 83(2-3):195–206, 2 2006. ISSN 03032647. doi: 10.1016/j.biosystems.2005.05.015.

Acknowledgments

We acknowledge the support of the Swiss National Science Foundation under Grant CRSII5_193740 and of the French Agence Nationale de la Recherche under grant ANR-21-CE30-0001 and Projet ANR-21-CE12-0023.

Author contributions

E.L. contributed to model development, performed simulations, analyzed data and interpreted results. F.D. contributed to model development and preliminary simulations. G.K. performed 1-bead-per-residue simulations and contributed data analysis. M.P. contributed to data analysis and interpretation. L.C. contributed to model development and interpretation. A.B. conceived and supervised the investigation, interpreting results and directing all contributions. E.L. and A.B wrote the manuscript, with contributions from all authors for editing and review.

Correspondence

Correspondence to Alessandro Barducci.